On the relationship between H2 addition, local extinction and hydrodynamic instability in non-premixed bluff-body stabilized flames

Kuppuraj Rajamanickam, Franck Lefebvre, Carole Gobin, Gilles Godard, Corine Lacour, Bertrand Lecordier, Armelle Cessou, David Honore

On the relationship between H_2 addition, local extinction and hydrodynamic instability in non-premixed bluff-body stabilized flames

Kuppuraj RAJAMANICKAM[1], Franck LEFEBVRE[1], Carole GOBIN[1], Gilles GODARD[1], Corine LACOUR[1], Bertrand LECORDIER[1], Armelle CESSOU[1], David HONORE *[1]

[1] CORIA-UMR 6614, CNRS, 76801 SAINT ETIENNE DU ROUVRAY CEDEX

*Corresponding author - david.honore@coria.fr

Keywords: Hydrogenated turbulent flames, Bluff Body burner, Time-resolved measurements, Simultaneous OH PLIF/PIV

ABSTRACT

We examined the effect of hydrogen (H_2) enrichment to methane (CH_4) in a non-premixed bluff-body stabilized burner operating under typical central jet dominated flame mode. In the chosen mode of operation, globally, the flow field and flame feature three important successive spatial regions, namely, recirculation zone, neck zone and jet-like flame zone. In such configuration, the flame is exposed to a higher stretch rate in the neck zone and eventually undergoes local extinction. Such local extinction and subsequent re-ignition of broken flame branches have strong implications over the hydrodynamic instability of the coaxial annular air shear layer. It is well known that H_2 addition increases the flame extinction strain rate and thus alters the local extinction phenomenon. To understand this phenomenon, we performed experiments at 10%, 20 %, 30% and 50 % hydrogen proportion in (H_2-CH_4) blend. High repetition rate (5 KHz) PIV and OH PLIF measurements are performed simultaneously to perceive the quantitative insights. The results obtained from POD and 1D wavelet transform indicated the suppression of vortex shedding at the annular air shear layer for H_2 addition greater than 20 %, and thus quantified the beneficial effect of H_2 addition in turbulent flame stabilization.

1. Introduction

The progressive rise in demand for clean combustion leads to increased interest in the development of power generation devices that can able to operate with low/zero-carbon fuels. Among the other options, hydrogen is emerging as a better candidate in the global mission of de-carbonization, as it can be readily produced from renewables such as wind and solar energy. Therefore, the usage of hydrogen as blended fuel with natural gas becomes an appealing strategy in the devices like gas turbines, high temperature furnaces, domestic burners etc. However, the difference in the thermophysical properties of H_2 in comparison to the conventional fuels possesses additional operational challenges. For instance, although the high flame speed together with a wide flammability range offer improved flame stabilization, however, it intensifies the risk of flashback (Ranjan and Clemens, 2021). Besides, the increased strain resistance due to H_2 enrichment (Shanbhogue et al., 2016) is expected to alter the flame shape significantly. Hence, it is

apparent that the widespread implementation of H_2 across various practical systems needs a thorough understanding of the various physical mechanisms. In this work, an experimental investigation has been carried out to understand the effect of H_2 addition to methane in the canonical non-premixed bluff body burner.

Many propulsive devices and stationary combustion facilities employ bluff body in the fuel injection system to improve flame stabilization. The flow field in the bluff body burner can be globally categorized into three regions namely, 1. Recirculation zone, 2. Neck zone, 3. Jet zone. The recirculation zone (RZ) is created at the exit of the burner thanks to the wake effect of the bluff body. It consists in a centripetal air vortex and a centrifugal fuel vortex that induces a partial premixing of a part of reactants. Downstream of the recirculation zone, flow converges towards the centerline and thereby increases the fluid dynamic strain in the neck zone. Consequently, the flame undergoes local extinctions sporadically in the neck zone. The local variation in the gas expansion ratio (T_b/T_u) caused by local extinctions is known to influence the hydrodynamics of the flow field. For instance, the experimental investigation by (Emerson et al., 2012) elucidated the influential feature of the density ratio in the absolute and convective instability transitions. Furthermore, the local extinctions in the reaction induce the entrainment of cold reactants into the hot wake region. Subsequently, the decrease in the density ratio has led the flow to become absolutely unstable (with asymmetric vortex shedding in the wake region) (Shanbhogue et al., 2009).

The objectives of this study are twofold. First, the impact of H_2 addition over the local extinction and subsequent re-ignition of the flame fronts in the neck zone is analyzed. The second objective is to demonstrate how these changes observed in local extinctions with respect to H_2 addition determine the evolution of large-scale coherent structures in the flow field. For this purpose, simultaneous high-speed PIV and OH-PLIF are implemented in a large part of the turbulent flame.

2. Experimental setup and test conditions

The non-premixed canonical bluff-body burner utilized in this study is depicted in **Figure 1**. It comprises of annular air passage and a central fuel injection port embedded with the cylindrical bluff body. The working fluids are air, methane, and hydrogen respectively. All the fluid flow rates are controlled using thermal mass flow meters (Bronkhorst). The fuel flow rates of CH_4 and H_2 are varied (**Table 1**) in reference to the control parameter namely, the volumetric concentration level of H_2 ($\boldsymbol{\alpha_{H2}}$) in the fuel blend while keeping constant the total thermal power of the burner. It should be noted that the annular airflow rate have been maintained constant across all the test conditions to separate the effect of H_2 addition to the main aerodynamic features

of the RZ controlled by the annular air flow (except in the case of F6, where the airflow rate is increased till lean blow-off limits). The time-averaged flow field pertains to F1 is presented in **Figure 1** b to illustrate the key aerodynamic features. Three distinct flow zones are identified. First region (Zone A) comprises of strong air recirculation zone (RZ) immediately downstream of the bluff body exit. Strictly speaking, there exists a small fuel recirculation zone induced between air RZ and central fuel jet, but it is rather very small/weak, hence the same is not explicitly marked in **Figure 1** b. Three shear layers are witnessed in Zone A, 1. Outer shear layer (OSL) formed between outer boundary of annular air jet and ambient; 2. Inner shear layer 1 (ISL1) separates the inner and outer boundaries of annular air jet and RZ respectively. 3. Inner shear layer 2 (ISL2) is induced between inner boundary of RZ and central fuel jet. More details on the influence of H_2 addition on the mean flame structure can be found in our previous work (Rajamanickam et al., 2021).

Table 1. Experimental conditions

(α_{H2})	Re_{fuel}	Re_{air}	Power (kW)	$MR=\left(\frac{\rho_{air}U_{air}^2}{\rho_{fuel}U_{fuel}^2}\right)$
0 (F1)	4370	10575	16.8	0.25
0.1 (F2)	4300	10575	16.8	0.26
0.2 (F3)	4218	10575	16.8	0.28
0.3 (F4)	4123	10575	16.8	0.31
0.5 (F5)	3872	10575	16.8	0.31
0.3 (F6)	4123	31725	16.8	2.77

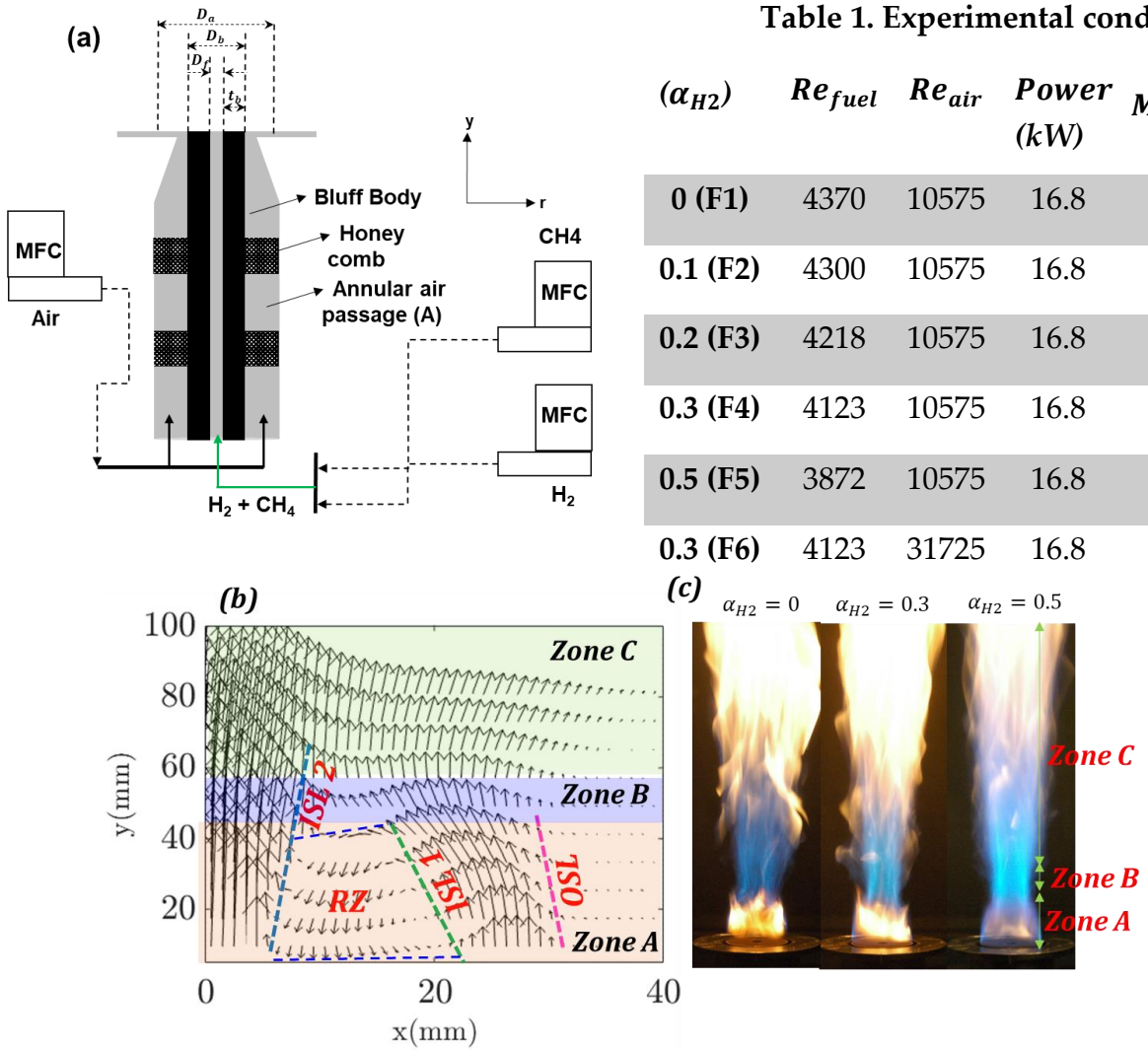

Figure 1. a. Configuration of canonical non-premixed bluff-body burner used in this study ($D_a = 55\ mm$; $D_b = 48\ mm$; $t_b = 20\ mm$); b – Time averaged flow field with distinct flow regions; c –Direct photographs of flames across various H_2 addition levels.

3. Laser diagnostics

Simultaneous high-speed PIV and OH PLIF are implemented at a repetition rate of 5 kHz. The configuration of the system is illustrated in **Figure 2**. The PIV system comprises of double cavity Nd: YAG laser (Photonics; λ~532 nm; 30 mJ/pulse; max rep rate – 10 kHz) and a CMOS camera (Phantom V2512). The laser beam is converted into a thin sheet of ~ 1mm thickness using a combination of spherical ($f = 1000\ mm$) and cylindrical lens ($f = -12\ mm$). Then the laser sheet is directed towards the longitudinal axis of the burner. Oxides of Zirconia particles are used as a tracing medium. It should be noted that, both the annulus air and fuel have been seeded separately. The Mie scattered light from the seeding particles are recorded using Phantom V2512 camera fitted with Nikon 105 mm lens.

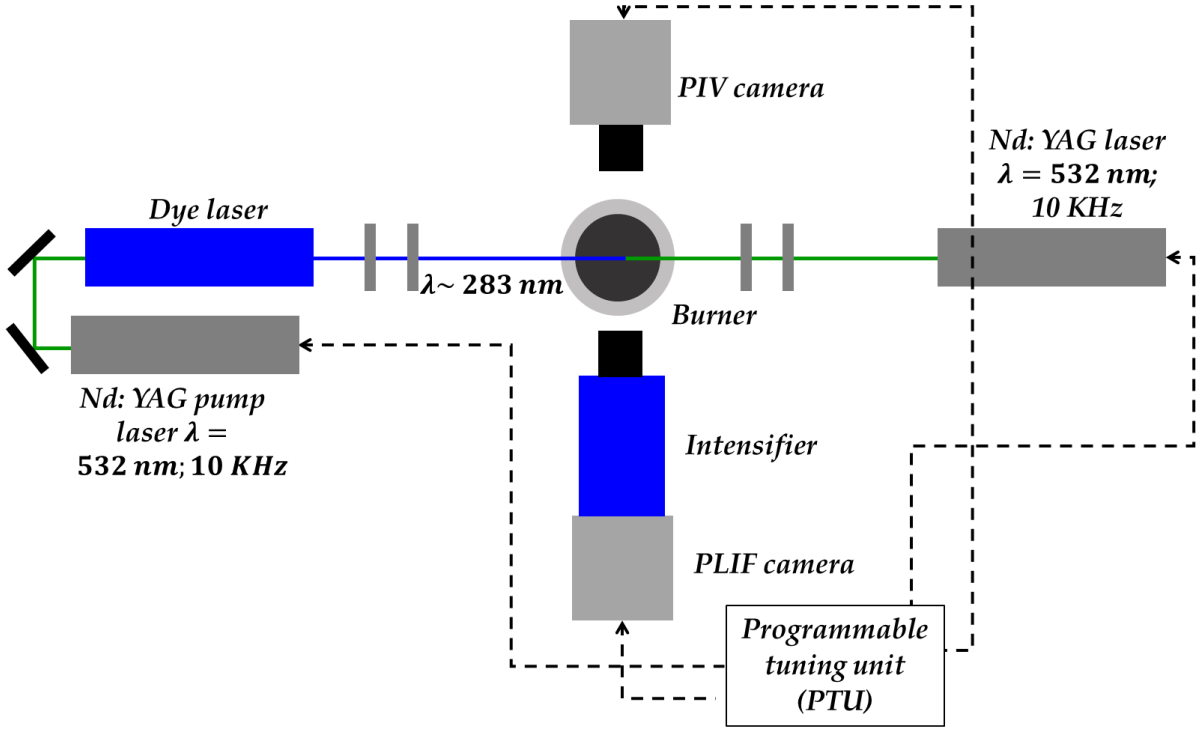

Figure 2. Schematic of time-resolved (5 kHz) simultaneous PIV and OH PLIF optical diagnostic systems

Besides, 532 nm bandpass filter is coupled with the lens to avoid flame emissions. The field of view for PIV measurements is chosen as 90 x 110 mm² and this yields a spatial resolution of 8.05 pixels/mm. The recorded images are post-processed in Lavision Davis 8.4 software to reconstruct the vector field. Across all the test cases, multipass decreasing interrogation window size with adaptive PIV scheme is employed. Accordingly, the initial and final interrogation window size has been chosen as 24 x 24 pixels and 16 x 16 pixels (with 50 % overlap) respectively. This results in the final vector spacing of 0.99 mm. The OH PLIF system (**Figure 2**) includes a Nd: YAG pump laser (Edgewave; λ~532 nm; max rep rate – 10 KHz) and a tunable dye laser (Sirah). The dye laser is tuned to produce a laser beam of wavelength ~ 566 nm with the help of Rhodamine 6G dye

dissolved with ethanol and then, it is frequency-doubled to get a desired UV laser beam of wavelength ~ 283 nm; 0.3 mJ/pulse. The generated 283 nm beam is used to excite the OH radicals in the Q1 (6) line of $A^2\sum+-X^2\prod(1,0)$ transition band. The UV laser beam is converted to a sheet of 0.5 mm thickness and approximately ~ 70 mm in height using sheet-making optics. Then it is aligned with the PIV laser sheet to acquire the OH fluorescence and flow field from the same longitudinal plane. Even if the pulse energy of the UV beam is very low, an illumination area of ~ 70 x 70 mm² is reached for PLIF imaging in the vertical plane, which enables to explore the whole of the A and B zones as well as the beginning of the zone C. Furthermore, the PLIF laser beam is temporally positioned between two PIV laser pulses to enable simultaneous acquisition of OH image and flow field.

The OH fluorescence intensity from the flame is captured using Photron SA5 camera coupled with a high-speed image intensifier (Make- LaVision). In addition to the UV lens (f / 2.8, 100 mm; Cerco), spectral filters UG11 and WG 305 are used in combination to avoid the Mie scattering from PIV tracers. The combination of spectral filtering and short gating (1500 ns) achieved through an intensifier facilitates the collection of OH fluorescence without the interference of flame emission. For all the test conditions, images are recorded at 5 kHz with an acquisition time of 2 secs. (i.e. 10000 images per test case). The resolutions of PIV and PLIF cameras at 5 KHz are 789 x 721pixels and 775 x 706 pixels respectively.

4. Image Processing

4.1. Step 1-Identification of holes

The first step is to identify the holes (aka –local extinctions) in the given set of instantaneous 2D HS - OH PLIF image series. To do this, an image-processing scheme based on the global thresholding approach has been implemented in MATLAB.

For better clarity, the working detail of the proposed image processing scheme is illustrated through two different instantaneous OH contours, one without a hole (**Figure 3** a) and another with a hole (**Figure 3** b). First, the raw OH PLIF image is converted into a binary image based on the user threshold. The resultant edges from the binary images are further smoothened using a Gaussian filter to avoid inaccuracies in the mapping of boundaries (step 1). We recommend the readers to refer (Kaiser and Frank, 2009) (Juddoo and Masri, 2011) for more details on this process. The image segmentation (step 2) algorithm helps to detect the objects in the resultant binarized images. For instance, the OH contour is unbroken in the image without local extinction (**Figure 3** a), hence only one object is detected. On the other hand, the spatial discontinuity occurred due to local extinction resulting in the detection of two objects (**Figure 3** b). Finally, the physical dimensions of the detected objects are retrieved using a bounding box (step 3).

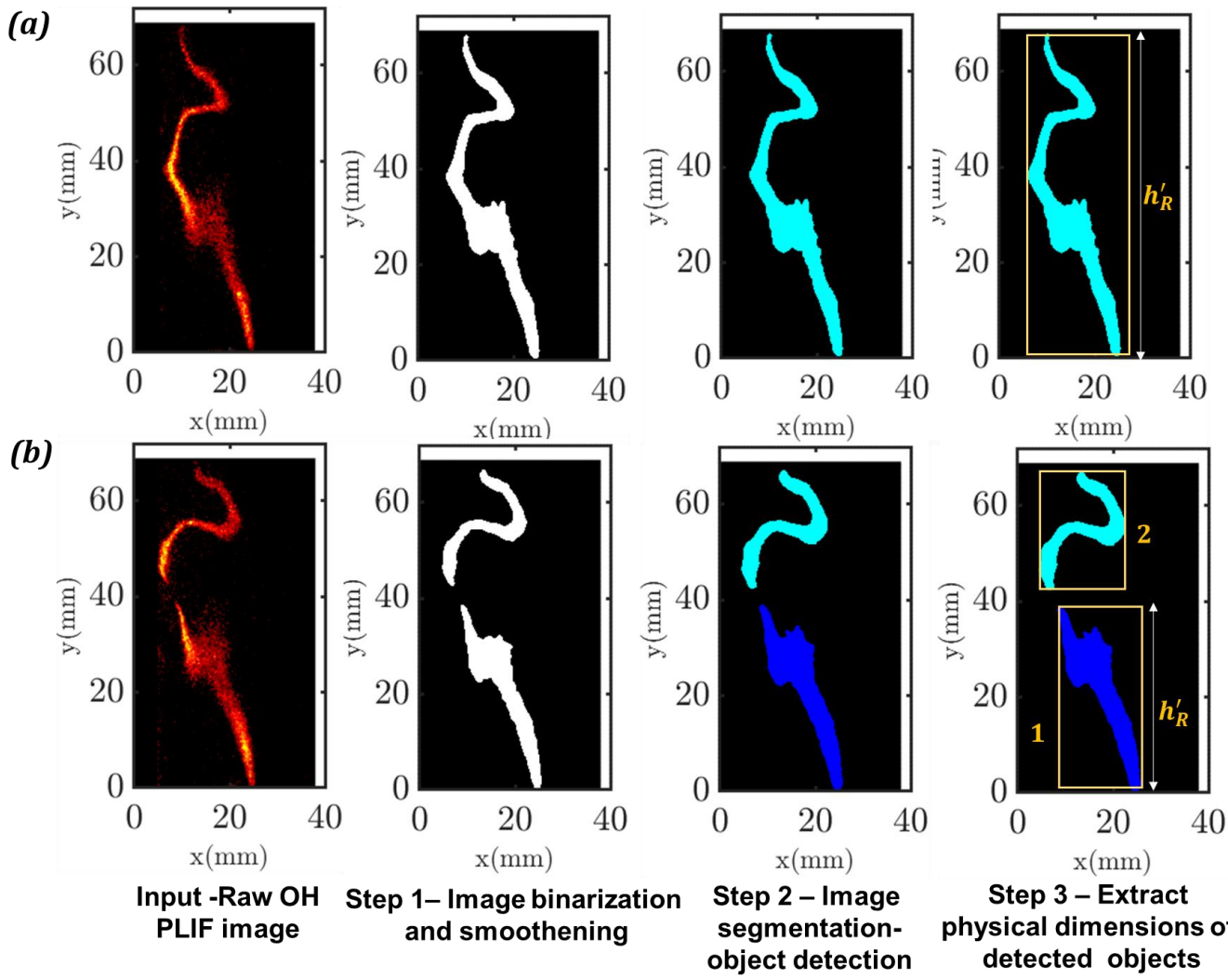

Figure 3. Steps involved in identification of holes in the 2D OH – PLIF image series.

4.2. Step 2- Temporal evolution of holes

Followed by local extinction, two major events namely closure and breakup are observed as depicted in **Figure 4**. Here, closure refers to the reconnection of the two branches in the subsequent time sequences after local extinction (**Figure 4b**) and vice versa refers to the breakup situation (**Figure 4**b). The bounding boxes are used to mark the boundaries of the two OH branches. The parameter 'y_h' that defines the distance between upper and bottom bounding boxes (aka - hole) is used to classify the closure and breakup events. For each event, five temporal sequences (i.e. 1 ms) are considered for understanding the time evolution of y_h. We have employed the similar procedure adopted by (Juddoo and Masri, 2011), accordingly the consecutive images that containing only the two OH branches formed after the local extinction in zone B are considered. This is because of the fact that during some time instants, additional OH islands could appear between the upper and lower branches initiating the re-ignition. These additional OH islands might be originated from the out-of-plane convection.

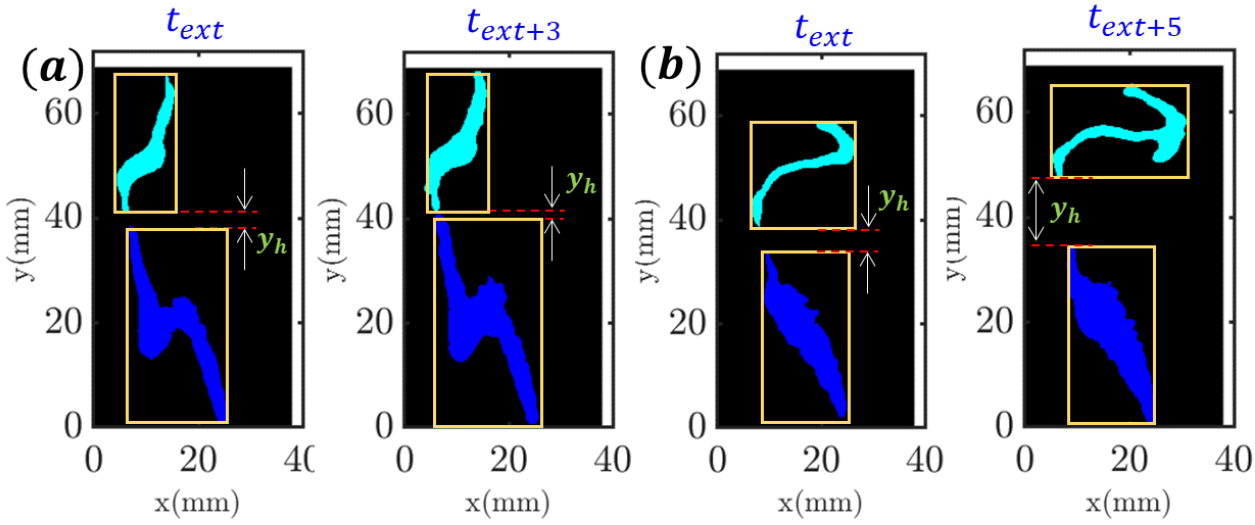

Figure 4 Schematic representation of closure (a) and breakup events (b)

5. Results

5.1 Influence of H_2 addition on hole formation and reconnection of holes

In the present study, holes are observed only for $0 \leq \alpha_{H2} \leq 0.3$. On contrary, despite the strong interaction of flame with annular airflow in the high strain neck zone, holes are not witnessed with $\alpha_{H2} \geq 0.5$. The increased H_2 enrichment level intensifies the extinction resistance of flame (κ_{ext}) (Shanbhogue et al., 2016) over the fluid dynamic strain (κ_{hyd}) and thereby prevents the occurrence of local extinction events. Moreover, the increase in flammability limits further prevents the local extinction even if the flame front encounters a sudden increase in diffusive flux due to the impingement of the central fuel jet vortex.

Since holes are not observed with the $\alpha_{H2} \geq 0.5$, as such the analysis briefed in **Figure 4** is not applicable for F5 case (i.e. $\alpha_{H2} \geq 0.5$). The histograms generated (**Figure 5** b) from the obtained values of y_h highlights the higher, lesser number of closure events for $\alpha_{H2} = 0.2, 0.3$ and $\alpha_{H2} = 0, 0.1$ respectively. This observation clearly delineates the favorable feature of H_2 addition over the reconnection of two OH branches within a shorter duration (i.e. < 1 ms). The closer inspection of the instantaneous data set reveals that, during closure events, either upward or downward movement of the upper/lower OH branch initiates the re-ignition. As inferred by (Juddoo and Masri, 2011), in the present study, the reconnection of a broken edge is predominately initiated by edge flame propagation mechanism. The conclusion on this is arrived at based on the criteria reported by (Steinberg et al., 2011) i.e. reconnection of two edges in a straight path. Yet the majority of sequential events observed during reconnection/closure shows the signature of edge flame propagation. For example, in the time sequences illustrated in **Figure 6** a, the reconnection of two branches largely takes place in a straight-line path confirming the significance of edge flame propagation.

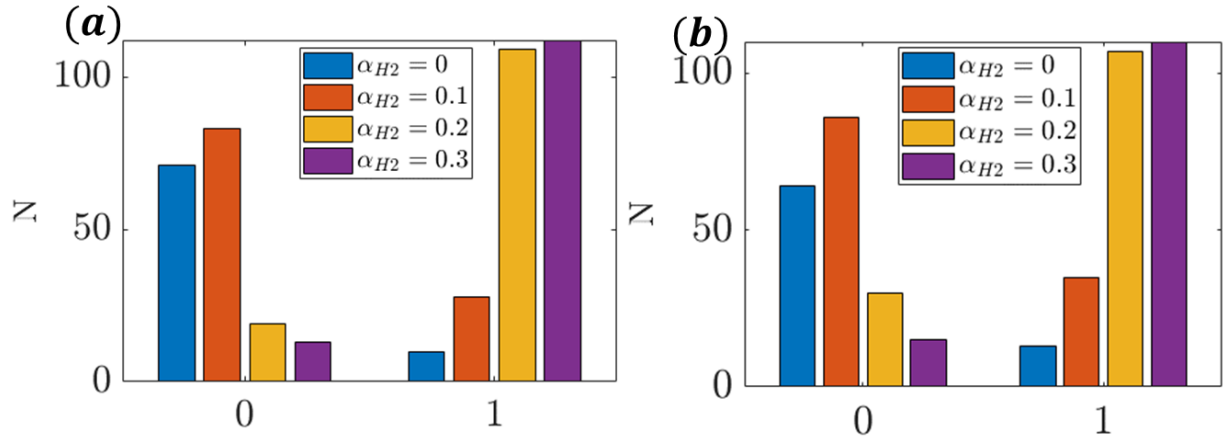

Figure 5 Histograms of breakup (0), and closure events (1) obtained across right (a) and left (b) side windows.

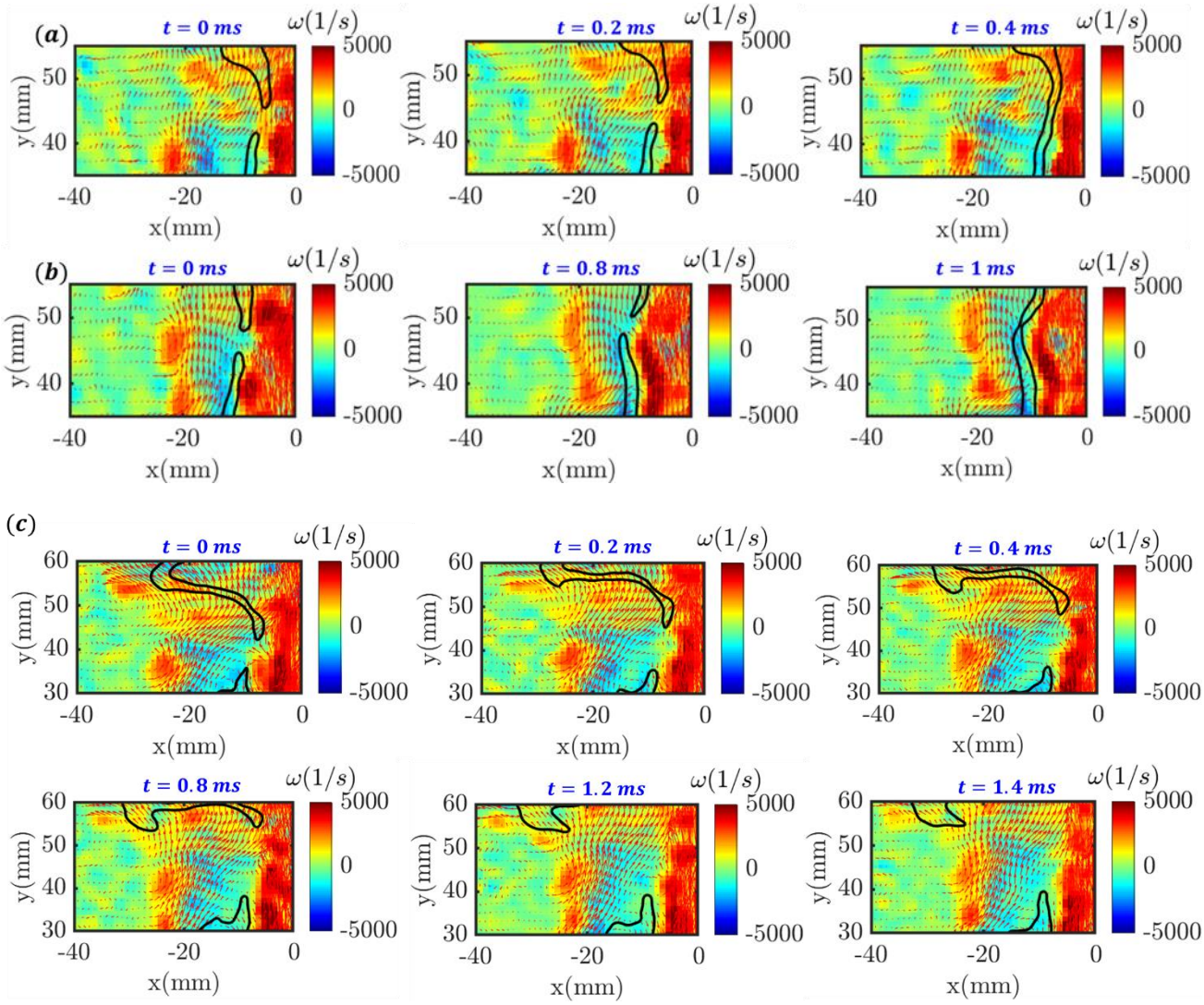

Figure 6. Typical time sequences illustrating the time evolution of locally extinguished flame fronts during re –ignition or breakup phase; a. $\alpha_{H2} = 0.1$; b. $\alpha_{H2} = 0$; **c.** $\alpha_{H2} = 0$

We did observed the role of surrounding turbulent eddies in the re-ignition process (**Figure 6** b; t = 0.8 ms), however, the final reconnection still happened due to edge flame propagation (**Figure 6** b; t = 1 ms). Moreover, in both the examples shown in **Figure 6**, the rapid displacement of edges by ~ 3 mm in the time interval of 0.2 ms further confirms the dominance of edge flame speed (U_{ed}) rather than the advection effect. In general, the edge flame speed is higher than the laminar flame speed (S_L) due to its propagation in the hot gases of unburned mixtures found in the vicinity of local extinction zone. (Im and Chen, 1999). (Ruetsch et al., 1995) proposed the theoretical expression for edge flame speed as follows, $U_{ed} \propto (\rho_u/\rho_b)^{0.5} . S_L$; where ρ_u/ρ_b represents the density ratio of burned and unburned mixtures. In the present study, the increase in density ratio as a result of higher local temperature can be interpreted from the observation of raise in OH intensity with H_2 addition. Furthermore, it is well known that H_2 addition leads to increase in the laminar flame speed (Dugger, 1952). Hence, rise in the edge flame speed (U_{ed}) by the combined effect of increase in laminar speed and density ratio might be a reason behind the higher probability of closure events witnessed with the test cases of $\alpha_{H2} = 0.2, \text{and } 0.3$.

On the other hand, the lesser edge flame speed associated with $\alpha_{H2} = 0$ and 0.1 results in failure of reattachment of the broken OH branches in a shorter duration, this essentially causes higher number of breakup events. During such breakup events, the lower part remains attached to the RZ, while, the upper part is progressively convected downstream by the coherent shedding vortices in the OSL. The time sequences (t = 0 – 1.4 ms) of the superimposed flow field and flame front boundaries shown in **Figure 6**c illustrate this phenomenon. Previous studies reported this periodic convection of the upper flame branch as split flashing (Chen et al., 1998) or moving fireballs/tubules (Roquemore et al., 1983). The lower branch that resides within the RZ is commonly referred to as residual flame (Zukoski, 1954).

5.2 Flow dynamics

Previous studies (Oberleithner et al., 2013) (Yin and Stöhr, 2020) showcased the influential feature of local extinction/reignition in the evolution of coherent structures in the flow field. Hence, the interplay between hole formation/reignition and flow field dynamics is explored in this section. To do this, Proper Orthogonal Decomposition (POD) has been implemented over the instantaneous data sets of PIV flow field to reveal the dominant energetic structures across the different operating conditions. We have implemented the method of snapshots POD (Sirovich, 1987) based on single value decomposition (SVD) (Kerschen et al., 2005). First, the temporal data sets are arranged into the big matrix U of $m \times n$, where the column n represents the instantaneous 2D data sets. POD analysis over the big matrix U essentially yields n eigen modes $\phi_j(x, y)$, temporal coefficients $a_j(t)$ and eigenvalues λ_j. Finally, the decomposed velocity fields u can be expressed as

$$\boldsymbol{u}\,(\boldsymbol{x},\boldsymbol{y},\boldsymbol{t_i}\,) = \sum_{\boldsymbol{j=1}}^{\boldsymbol{N}} \boldsymbol{a_j}\,(\boldsymbol{t_i}\,)\;\boldsymbol{\phi_j}\,(\boldsymbol{x},\boldsymbol{y})$$

Where, $\boldsymbol{t_i}$ – time instant of the original data; j- mode number; N – total number of instantaneous data sets.

Figure 7 represents the first four dominant spatial modes retrieved from the PIV flow fields. Here, the spatial modes are visualized using vorticity contours. All the four modes of $\alpha_{H2} = 0, 0.1$ shows the dominance of large-scale vortex shedding at OSL just downstream of RZ. Besides, the appearance of coherent structures in the region of 30 mm < y < 50mm; -15 mm < x < -15 mm highlights the strong interaction of the annular jet with the central fuel jet in the neck zone (Zone B). The dominance of vortex shedding modes with $\alpha_{H2} = 0, 0.1$ can be interpreted as an interlink between the local extinction and subsequent increase in the entrainment of the fresh reactants (within RZ) due to the failure of reconnection of flame branches as discussed in section 5.2. Many researchers (Nair and Lieuwen, 2007) (Kiel et al., 2007) (Shanbhogue et al., 2009) reported the emergence of an asymmetric sinuous mode of wake oscillations in the bluff body stabilized flames that exhibited higher probability of local extinction events. For instance, the experiments carried out by (Nair and Lieuwen, 2007) in the near blow-off bluff-body flames reveal, increase in the localized extinction events leading to significant alteration of wake dynamics, and irregular wrinkling of the flame fronts. They also found that these large-scale oscillations in the wake possess characteristic features similar to the classical Bénard – Von Karman (BVK) instability that normally presents in non-reacting bluff body flows. In general, BVK instability is often suppressed in reacting flows due to the presence of large density gradients in the shear layer (McMurtry et al., 1989) (Soteriou and Ghoniem, 1994). However, in the cases of flames close to blow off (i.e. *the one with a higher degree of local extinctions*), the decrease in the density ratio (ρ_u/ρ_b) leads to reemergence of BVK instability in the shear layer (Smith et al., 2007). In line with this argument, as in the case of $\alpha_{H2} = 0, 0.1$, the lesser probability of flame presence in the region beyond y > 30 mm as consequence of failure of reconnection of holes resulted in drop in density gradients and thus dominance of vortex shedding.

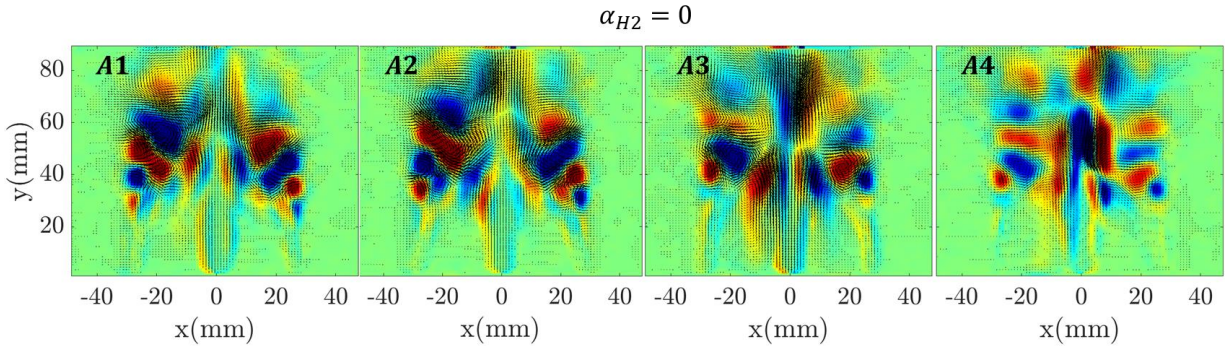

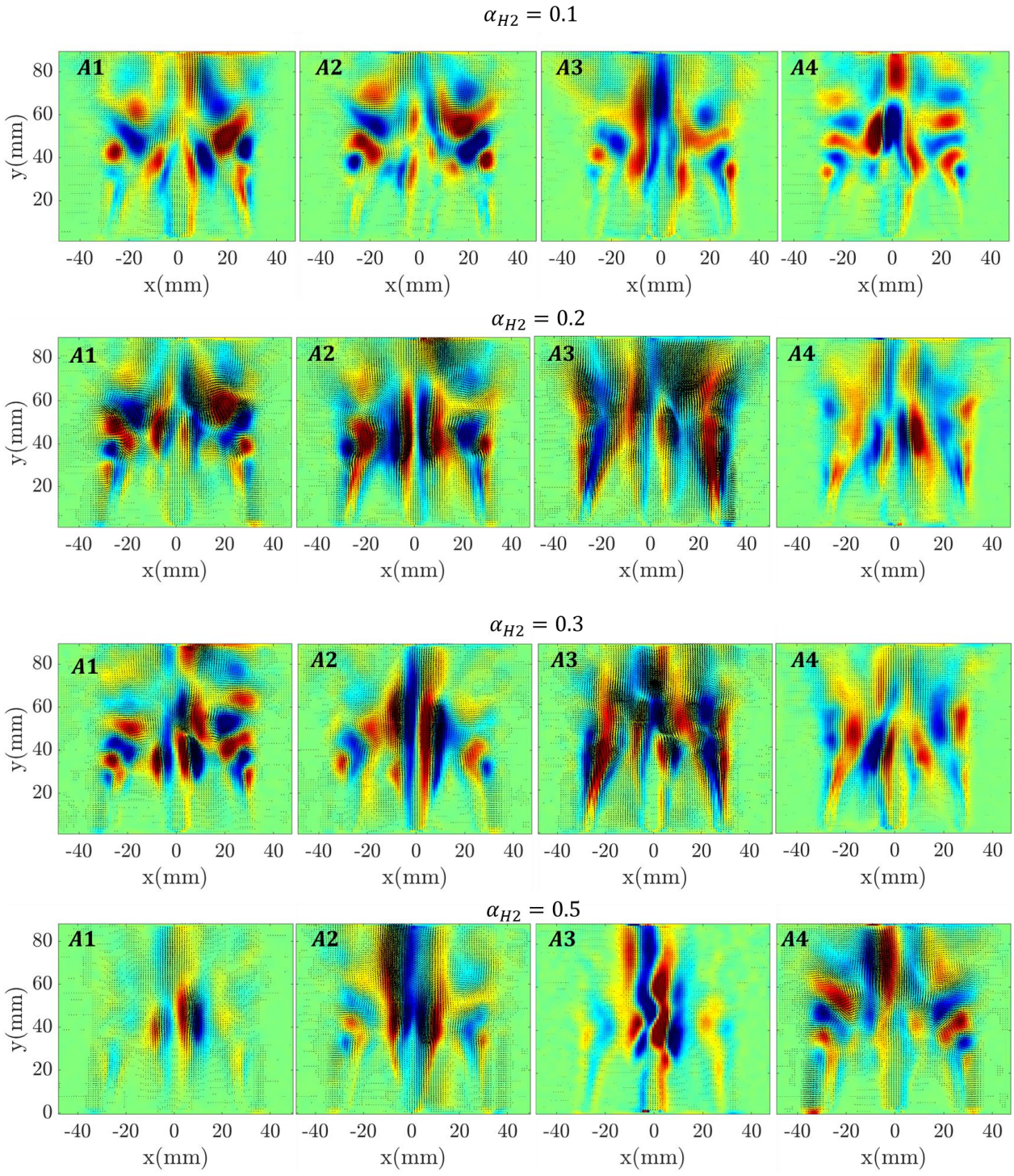

Figure 7 Evolution of spatial POD modes across different H_2 addition levels

The experimental investigation carried out by (Emerson et al., 2012) in the premixed bluff body flames reveals a transition from global BVK (*vortex shedding*) to convective Kelvin-Helmholtz (KH) instability at higher density ratios. They also reported intermittency in the switching of flow states between KH and BVK instability modes even at fixed operating conditions. We have observed such scenario in the test cases of $\alpha_{H2} = 0.2, 0.3$, i.e. only the first two modes (A1, A2) in

$\alpha_{H2} = 0.2, 0.3$ shows the dominance of vortex shedding in OSL. The other two modes (i.e. A3, A4) exhibit the spatial structures similar to the KH/shear instability i.e. over here the alternate pattern of vortices are absent at the OSL.

The reconstructed instantaneous flow fields based on POD modes (only with the first 10 modes) suggests the dominance of vortex shedding for $\alpha_{H2} = 0, 0.1$ and periodic switching between vortex shedding, and KH for $\alpha_{H2} = 0.2, 0.3$. To further elucidate the role of vortex shedding and periodic switching phenomenon, we have implemented a 1D continuous wavelet transform (CWT). CWT is chosen instead of FFT on POD time coefficients because the former allows us to characterize the system that is oscillating between different dynamic states. Here, CWT has been applied over the instantaneous vorticity values extracted from the small vector region of 7 x 7. The chosen region is located at the OSL where the vortex shedding is prominent. In the present study, wavelet transform is computed using the 1D CWT function available in MATLAB. More details on the used CWT function can be found in (Torrence and Compo, 1998).

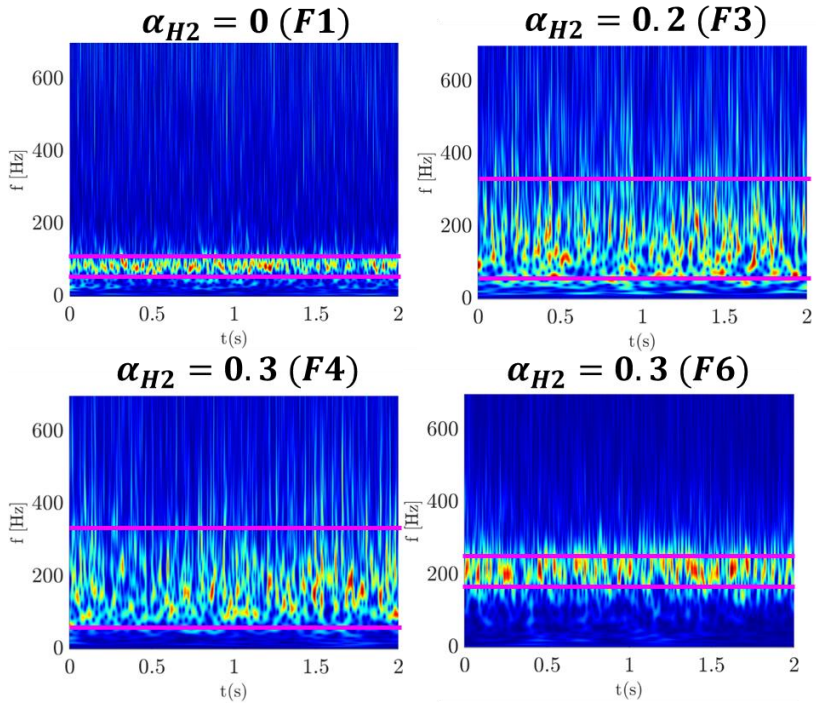

Figure 8. Magnitude of frequency spectrum scalograms obtained from CWT

The results obtained across the left and right side of the OSL depicts a similar feature, hence, for brevity, only the CWT scalogram pertaining to the right side is shown here (**Figure 8**). For test cases $\alpha_{H2} = 0, 0.1$, the frequency values are prominently concentrated at ~ 85 Hz (**Figure 8**). Furthermore, the obtained frequency corresponds to a Strouhal number ($St = ft_b/U_b$) of 0.25, which is known to be characteristic frequency of vortex shedding (Prasad and Williamson, 1997). Hence, the results of CWT confirm the domination of vortex shedding phenomenon during $\alpha_{H2} = 0, 0.1$ operating conditions. On the other hand, the frequency spectrum shows broadband features for $\alpha_{H2} = 0.2, 0.3$ and intermittently oscillating between 50 to 250 Hz. Such intermittent

oscillations delineate the periodic switching of flow between different instability modes (e.g. vortex shedding and KH). These observations are consistent with the results of (Emerson et al., 2012) (Erickson and Soteriou, 2011), where they have reported the occurrence of narrow-band oscillations in the flames with lower density ratio and vice versa for higher density ratio/temperature ratio flames. In order to further access this phenomenon, experiments are conducted at varying level of air flow rates for $\alpha_{H2} = 0.3$. Interestingly, the obtained spectrogram for the case that is close to blow off exhibit narrow band even with 30 % H_2 (F6) addition. This is because the intensification of location extinction events due to increased annular air flow rate indeed results in the re-emergence of BVK instability.

6. Conclusion

The impact of H_2 addition in the non-premixed bluff-body stabilized turbulent flames have been studied using simultaneous time-resolved PIV and OH - PLIF. Such measurements enabled us to explore the links between H_2 addition, local extinction /reignition and hydrodynamic instability. The canonical non-premixed bluff-body burner is operated with increasing levels of H_2 addition (10%, 20%, 30%, 50%). The increased extinction strain resistance of the flame with H_2 enrichment led to an absence of local extinctions/holes in the flame sheet for $\alpha_{H2} \geq 0.5$. The 10% H_2 addition (F2 case) doesn't show any improvements with the re-ignition of holes in comparison to 0% H_2 (F1). However, both 20% (F2) and 30% (F3) presents significant modifications in the re-ignition of holes. The closer inspection of the instantaneous 2D OH PLIF images delineates the re-connection of holes are majorly initiated by edge flame propagation. Next, POD and 1D CWT are implemented over the time-resolved PIV data to gain insights into the evolution of coherent structures in the flow field. Vortex shedding induced by BVK instability is observed across all the modes in the 0% and 10% H_2 addition, contrarily, the dominant modes are found to be oscillating between KH and BVK modes with H_2 = 20 %, 30%. This suggests that local variation in the temperature ratio (T_b/T_u) caused by H_2 addition indeed influences the hydrodynamics of the flow field.

Acknowledgements

This project has received funding from Région Normandie (project name-RAPHYD; Grant RIN 2018) under the framework of EU's regional development fund (ERDF).

References

Chen, Y., Chang, C., Pan, K.-L., Yang, J.-T., 1998. Flame lift-off and stabilization mechanisms of nonpremixed jet flames on a bluff-body burner. Combustion and flame 115, 51–65.

Dugger, G.L., 1952. Effect of initial mixture temperature on flame speed of methane-air, propane-air and ethylene-air mixtures. US Government Printing Office.

Emerson, B., O'Connor, J., Juniper, M., Lieuwen, T., 2012. Density ratio effects on reacting bluff-body flow field characteristics. Journal of Fluid Mechanics 706, 219–250.

Erickson, R.R., Soteriou, M.C., 2011. The influence of reactant temperature on the dynamics of bluff body stabilized premixed flames. Combustion and Flame 158, 2441–2457.

Im, H.G., Chen, J.H., 1999. Structure and propagation of triple flames in partially premixed hydrogen–air mixtures. Combustion and flame 119, 436–454.

Juddoo, M., Masri, A.R., 2011. High-speed OH-PLIF imaging of extinction and re-ignition in non-premixed flames with various levels of oxygenation. Combustion and Flame 158, 902–914.

Kaiser, S.A., Frank, J.H., 2009. Spatial scales of extinction and dissipation in the near field of non-premixed turbulent jet flames. Proceedings of the Combustion Institute 32, 1639–1646.

Kerschen, G., Golinval, J., Vakakis, A.F., Bergman, L.A., 2005. The method of proper orthogonal decomposition for dynamical characterization and order reduction of mechanical systems: an overview. Nonlinear dynamics 41, 147–169.

Kiel, B., Garwick, K., Gord, J., Miller, J., Lynch, A., Hill, R., Phillips, S., 2007. A detailed investigation of bluff body stabilized flames, in: 45th AIAA Aerospace Sciences Meeting and Exhibit. p. 168.

McMurtry, P.A., Riley, J.J., Metcalfe, R.W., 1989. Effects of heat release on the large-scale structure in turbulent mixing layers. Journal of Fluid Mechanics 199, 297–332.

Nair, S., Lieuwen, T., 2007. Near-blowoff dynamics of a bluff-body stabilized flame. Journal of Propulsion and power 23, 421–427.

Oberleithner, K., Terhaar, S., Rukes, L., Oliver Paschereit, C., 2013. Why nonuniform density suppresses the precessing vortex core. Journal of Engineering for Gas Turbines and Power 135.

Prasad, A., Williamson, C.H., 1997. The instability of the shear layer separating from a bluff body. Journal of fluid mechanics 333, 375–402.

Rajamanickam, K., Lefebvre, F., Gobin, C., Godard, G., Lacour, C., Lecordier, B., Cessou, A., Honoré, D., 2021. Insights into the dynamics of local flame extinction events in CH4-H2 turbulent flames, in: European Combustion Meeting 2021.

Ranjan, R., Clemens, N.T., 2021. Insights into flashback-to-flameholding transition of hydrogen-rich stratified swirl flames. Proceedings of the Combustion Institute 38, 6289–6297.

Roquemore, W.M., Britton, R.L., Sandhu, S.S., 1983. Dynamic behavior of a bluff-body diffusion flame. AIAA journal 21, 1410–1417.

Ruetsch, G.R., Vervisch, L., Linán, A., 1995. Effects of heat release on triple flames. Physics of Fluids 7, 1447–1454.

Shanbhogue, S.J., Husain, S., Lieuwen, T., 2009. Lean blowoff of bluff body stabilized flames: Scaling and dynamics. Progress in Energy and Combustion Science 35, 98–120.

Shanbhogue, S.J., Sanusi, Y.S., Taamallah, S., Habib, M.A., Mokheimer, E.M.A., Ghoniem, A.F., 2016. Flame macrostructures, combustion instability and extinction strain scaling in swirl-stabilized premixed CH4/H2 combustion. Combustion and Flame 163, 494–507.

Sirovich, L., 1987. Turbulence and the dynamics of coherent structures. I. Coherent structures. Quarterly of applied mathematics 45, 561–571.

Smith, C., Nickolaus, D., Leach, T., Kiel, B., Garwick, K., 2007. LES blowout analysis of premixed flow past V-gutter flameholder, in: 45th AIAA Aerospace Sciences Meeting and Exhibit. p. 170.

Soteriou, M.C., Ghoniem, A.F., 1994. The vorticity dynamics of an exothermic, spatially developing, forced, reacting shear layer, in: Symposium (International) on Combustion. Elsevier, pp. 1265–1272.

Steinberg, A.M., Boxx, I., Arndt, C.M., Frank, J.H., Meier, W., 2011. Experimental study of flame-hole reignition mechanisms in a turbulent non-premixed jet flame using sustained multi-kHz PIV and crossed-plane OH PLIF. Proceedings of the Combustion Institute 33, 1663–1672.

Torrence, C., Compo, G.P., 1998. A practical guide to wavelet analysis. Bulletin of the American Meteorological society 79, 61–78.

Yin, Z., Stöhr, M., 2020. Time–frequency localisation of intermittent dynamics in a bistable turbulent swirl flame. Journal of Fluid Mechanics 882.

Zukoski, E.E., 1954. Flame stabilization on bluff bodies at low and intermediate Reynolds numbers (PhD Thesis). California Institute of Technology.